Simultaneous acquisition of the real and imaginary components in Fourier domain optical coherence tomography using harmonic detection

Andrei B. Vakhtin*, Daniel J. Kane and Kristen A. Peterson
Southwest Sciences, Inc., 1570 Pacheco St., Suite E-11, Santa Fe, New Mexico 87505

ABSTRACT

Fourier domain optical coherence tomography (FD-OCT) is an interferometric imaging technique that allows imaging to depths of a few mm in scattering biological tissues with high resolution of the order of 1-10 μm. However, the usefulness of FD-OCT is limited by background and autocorrelation interference terms that reduce the sensitivity and by phase ambiguity that halves the useful imaging depth range. These limitations can be overcome by obtaining the full, complex spectral interferogram. Simultaneous detection of the imaginary and real terms is obtained by phase modulating the reference arm of the interferometer and detecting at the first and second harmonics. A mathematical derivation of harmonically detected FD-OCT and experimental measurements showing that phase ambiguity artifacts can be suppressed by up to 70 dB are presented. The method provides efficient suppression of the complex conjugate, dc, and autocorrelation artifacts and has low sensitivity to phase noise. Beyond the removal of artifacts, the ability to obtain the full, complex interferogram is key to the development of spectrally resolved FD-OCT which would add depth-resolved spectroscopic detail to the structural information.

Keywords: optical coherence tomography, interferometry, biomedical imaging, harmonic detection

1. INTRODUCTION

Optical coherence tomography (OCT) uses low-coherence optical interferometry to obtain high-resolution, depth-resolved 2 and 3-dimensional images in scattering materials such as biological tissues. Time domain OCT (TD-OCT) is related to optical coherence reflectometry, where the optical phase delay of light scattered from different depths within a sample is measured by scanning the optical path length of the reference arm of an interferometer. Fourier domain OCT (FD-OCT) is a related technique based on spectral interferometry. In this case, the reference and sample arms of an interferometer remain stationary and the output of the interferogram is spectrally resolved. Fringes on the output spectrum result from light scattering from different depths in the sample and Fourier transform provides the depth profile. In both cases, the low coherence of the light source provides a "coherence gate" for depth resolution. FD-OCT has been implemented in two ways: (1) a multi-element array detector can be used to obtain the spectrally resolved (spectral) interferogram, providing simultaneous acquisition of data from each depth in the sample, and (2) a light source that can be rapidly tuned across a wide spectral range is used with a single element detector. This second implementation is known as swept source OCT.

During the past few years, FD-OCT has become an attractive alternative to conventional TD-OCT because it has been demonstrated, both theoretically and experimentally, that FD-OCT has the potential to provide better sensitivity than TD-OCT[1-3] and high speed versions of FD-OCT have been developed. However, a major drawback of FD-OCT that limits its practical use is the complex conjugate ambiguity, which is inherent to real Fourier transforms. This is a problem not present in TD-OCT. Because of this artifact, an FD-OCT image obtained from a real valued spectral interferogram is always symmetrical with respect to the zero plane (zero phase delay) of the interferometer. To avoid ambiguity in interpretation of the image, the zero plane must be positioned outside of the imaged sample. Thus, only one half of the imaging depth range is useful in practice. Resolving the complex conjugate ambiguity would double the imaging depth range and provide additional flexibility by allowing arbitrary positioning of the zero plane, *e.g.*, moving it inside the sample. Placement of the zero plane within the sample can allow imaging to greater depths, provided that sufficient light is returned from the sample.

*avakhtin@swsciences.com; phone 1 505 984-1322; www.swsciences.com

Smart Medical and Biomedical Sensor Technology IV, edited by Brian M. Cullum, J. Chance Carter
Proc. of SPIE Vol. 6380, 63800N, (2006) · 1605-7422/06/$15 · doi: 10.1117/12.685400

Ideally, the full complex spectral interferogram should be obtained in FD-OCT to take advantage of additional information contained within the data. This not only eliminates the complex conjugate artifact but also prevents loss of potentially valuable spectroscopic information. In fact, it is the access to both real and imaginary parts of the spectral interferogram that makes FD-OCT a true Fourier-transform analog of TD-OCT. It is essential to be able to obtain the complex interferogram for the development of spectroscopically resolved FD-OCT, where depth resolved spectral information is obtained concurrent with structural detail.[4,5] While TD-OCT, in principle, can provide the spectroscopic information in addition to structural information, the full interferogram must be digitized, requiring high-bandwidth electronics.[6] Generally, in TD-OCT, only the envelope of the interferogram is detected. The FD-OCT method may be more appropriate for spectroscopic OCT due to lower bandwidth requirements. However, full complex interferograms have to be acquired in order to extract the correct spectroscopic information.

Recently, several different approaches have been developed to address the problems of obtaining the full complex interferogram and resolving the complex conjugate ambiguity in FD-OCT. These include phase stepping methods,[7-10] simultaneous detection of the quadrature components of the interferogram by using 3×3 fiber-optic couplers,[11,12] separation of the two complex conjugate images using carrier frequency shifting in swept-source FD-OCT,[13-15] and using polarization-based optical demodulation.[16] Phase stepping methods[7,8] allow acquisition of the complex spectral interferogram to be obtained in a multi-frame sequence of reference arm phase shifts. However, in practice the complex conjugate rejection ratio is limited by the accuracy of the phase steps and also by the mechanical stability of the interferometer and the sample during the acquisition time of the frame sequence.[9,10] Although least-squares algorithms are somewhat helpful in determining the actual phase step amplitudes,[17,18] the rejection of the complex conjugate is usually < 40 dB.

The use of 3 × 3 fiber couplers as phase-shifting elements allows simultaneous detection of the real and imaginary components of the spectral interferogram by two separate detectors.[11,12] However, slight misalignments in matching the spectrometers (in the case of broadband FD-OCT) and uneven wavelength-dependent splitting ratios in the coupler that lead to imperfect subtraction of the spectra (in the case of swept source OCT) limit the suppression of the complex conjugate artifacts. The reported maximum complex conjugate rejection ratio is 20 dB for broadband FD-OCT and 30 dB for swept source OCT.[12]

Carrier frequency shifting methods in swept-source OCT separate the two mirror images and resolve the complex conjugate ambiguity.[13-15] However, these methods are not applicable to broadband FD-OCT which involves detection of the spectral interferograms with an array detector. Recently, a complex conjugate rejection ratio of >50 dB has been reported for the polarization-based optical demodulation method.[16] However the technique appears to be sensitive to environmental variations. Also, it is not clear how birefringence of the sample affects the performance of the method.

We have developed a new, alternative method of direct acquisition of the complex spectral interferogram that requires only a simple modification to broadband FD-OCT instrumentation and should also be straightforward to implement with swept source OCT. The imaginary and real components are detected simultaneously as the first and second harmonics of a phase-modulated interferogram. A distinct advantage over phase stepping methods is that the phase shift does not need to be accurately known. Previously, we demonstrated that the method efficiently removes the dc, autocorrelation, and complex conjugate artifact by imaging a one-surface sample (a mirror) using a scanning monochromator to obtain the spectral interferogram.[19] Even with that very slow acquisition method, the measured complex conjugate rejection ratio was at least 45 dB and was limited by the background noise floor. In this paper we present a more detailed description of the method and show complex-conjugate-resolved FD-OCT images of more complex samples including multi-surface test targets and a *Xenopus Laevis* tadpole using an array detector to capture the complex spectral interferogram. Complex conjugate rejection ratios of up to 70 dB are observed.

2. EXPERIMENTAL METHODS

A schematic diagram of the experimental setup used in this demonstration is shown in Fig. 1. The setup is based on a Michelson-type interferometer. The reference arm is phase modulated at 23 Hz with a sine wave applied to the piezo translator holding the reference mirror. The amplitude of the phase modulation is arbitrary and quite small, ~ 1 radian. In the experiments reported here, the modulation amplitude determined by optimizing the rejection ratio as described in Section 3 is 2.63 radians. A dual super luminescent diode (SLD) light source emitting at 1300 nm (bandwidth 85 nm) is used (Superlum Broadlighter 1300). The sample arm light beam is focused onto the sample, providing point

illumination. Phase modulated spectral interferograms are acquired at a rate of 200 Hz at each point using a 16 bit, 512-element linear InGaAs integrating array detector (Hamamatsu C8061) coupled to a spectrometer and digitized to a personal computer. Typically, 400 sequential interferograms are acquired at each point, providing a wavelength resolved, phase modulated signal. The signal at each wavelength is digitally demodulated at the first and second harmonics to obtain the real and imaginary parts of the interferogram. The inverse Fourier transform applied to the complex spectral interferogram produces the complex time domain depth profile (A-scan) where the DC and autocorrelation terms, and the complex conjugate artifact are suppressed. The effective A-scan acquisition rate is 0.5 Hz. Two-dimensional images consisting of multiple A-scans are obtained by using an optical scanner.

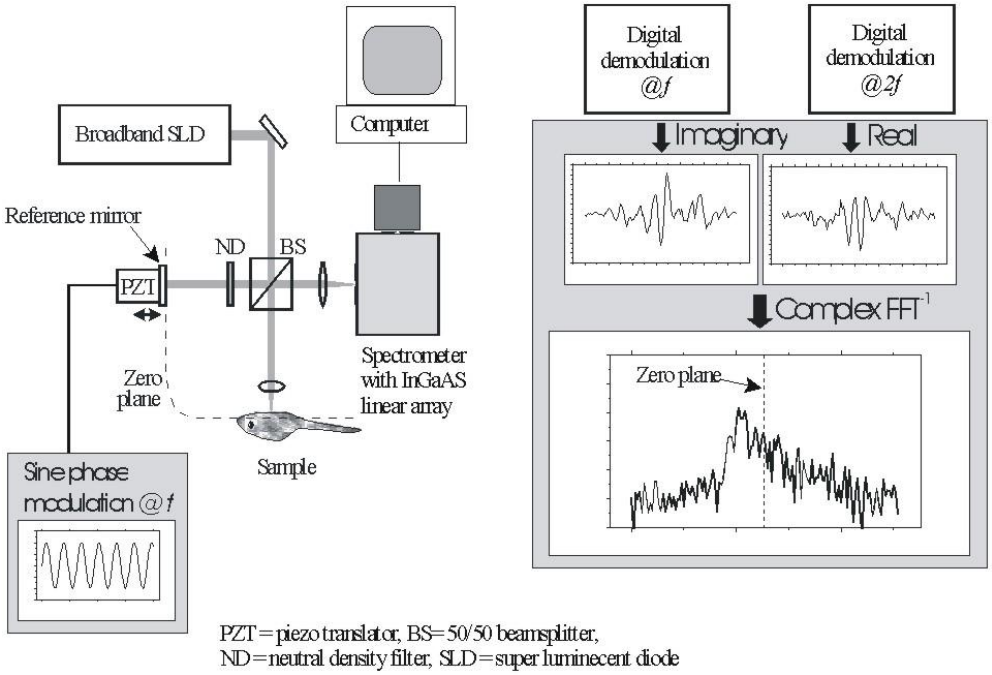

Fig. 1 Experimental schematic.

3. HARMONICALLY DETECTED COMPLEX FD-OCT

The spectral interferogram at the output of the interferometer under stationary conditions (no phase modulation) can be expressed as follows:

$$I_{SI}(\omega,\phi(\omega)) = I_R(\omega) + I_S(\omega) + 2\sqrt{I_R(\omega)I_S(\omega)}\cos(\phi_S(\omega) - \phi_R(\omega) - \phi(\omega)) \quad (1)$$

where ω is the frequency of the electromagnetic wave; $I_{SI}(\omega,(\phi(\omega))$ is the frequency- and phase-dependent spectral interferogram; $\phi(\omega)$ is a fixed frequency-dependent phase delay at the output of the interferometer; $I_R(\omega)$ and $\phi_R(\omega)$, and

$I_S(\omega)$ and $\phi_S(\omega)$ are the light intensities and phases in the reference and the sample arms of the interferometer, respectively. When a harmonic phase modulation is applied, the phase delay $\phi(\omega)$ becomes time dependent:

$$\phi(\omega) = \phi_0(\omega) + a_m(\omega)\sin\omega_m t \tag{2}$$

Here t is the time, $\omega_m = 2\pi f$ is the phase modulation frequency, and $a_m(\omega)$ is the modulation amplitude.

By calculating the Fourier components of the phase-modulated interferogram we can express the signals demodulated at the first (H_1) and second (H_2) harmonic as follows:

$$H_1(\omega,\phi_0(\omega)) = 4J_1(a_m(\omega))\sqrt{I_R(\omega)I_S(\omega)}\sin(\phi_S(\omega) - \phi_R(\omega) - \phi_0(\omega)) \tag{3}$$

$$H_2(\omega,\phi_0(\omega)) = -4J_2(a_m(\omega))\sqrt{I_R(\omega)I_S(\omega)}\cos(\phi_S(\omega) - \phi_R(\omega) - \phi_0(\omega)) \tag{4}$$

where $J_1(a_m(\omega))$ and $J_2(a_m(\omega))$ are the first- and second-order Bessel functions. Equations (3) and (4) represent the imaginary and real components of the complex spectral interferogram, respectively. The complex inverse Fourier transform can be applied to the complex spectral interferogram to convert it into the time domain depth profile that is free from the complex conjugate ambiguity, and also the DC and autocorrelation terms:

$$f(\tau) = \Im^{-1}\{-\beta H_2(\omega,\phi_0(\omega)) + iH_1(\omega,\phi_0(\omega)\} \tag{5}$$

β is equal to

$$\beta = J_1(a_m(\omega))/J_2(a_m(\omega)) \tag{6}$$

and depends only on the modulation amplitude a_m which is, generally, wavelength dependent. For example, if the phase modulation is achieved by dithering the reference mirror, a_m scales linearly with the optical frequency ω, which can easily be taken into account during signal acquisition and signal processing.

In practice, it is not necessary to know a_m precisely, β can be treated as an adjustable parameter using the following procedure: First, the initial setup of the instrument has to be performed. It consists of the following steps:

1. With a mirror used as a sample, the interferograms demodulated at the first and the second harmonics are acquired, and the phases are adjusted so that one of the quadrature components (sine or cosine) for each of the demodulated signals is maximized.

2. An initial value of the modulation amplitude a_m^0 is assumed.

3. The modulation amplitudes $a_m(\omega_i)$ are calculated for each optical frequency ω_i of the acquired spectral interferogram. In our case, where the phase modulation is achieved by dithering the reference mirror, a_m scales linearly with the optical frequency ω: $a_m(\omega_i) = a_m^0\omega_i / \omega_0$, where ω_0 is the center optical frequency of the spectral window.

4. The scaling coefficients β are calculated for each optical frequency ω_i of the acquired spectral interferogram according to eq. 6: $\beta(\omega_i) = J_1(a_m^0\omega_i / \omega_0)/J_2(a_m^0\omega_i / \omega_0)$.

5. The inverse complex Fourier transform is applied to the scaled complex interferogram (see eq. 5) to obtain the time domain depth profile — A-scan.

6. From the A-scan, the complex conjugate artifact rejection ratio is determined.

7. If a satisfactory complex conjugate rejection ratio is achieved, the initial setup is finished. If not, the sequence starting from Step 3 is repeated with a new approximation for a_m^0.

After the initial setup is complete, the instrument can be used for imaging other samples. The initial setup has to be performed only once for a given set of experimental conditions. Our experience shows that as long as the modulation amplitude and the set of optical frequencies for spectral interferogram acquisition are not changed, it is not necessary to re-run the initial setup.

By using phase modulation and demodulating the wavelength-resolved signal at the first and second harmonics, the quadrature components of the complex differential spectral interferogram can be simultaneously detected. This method provides efficient rejection of the DC and autocorrelation terms and resolves the complex conjugate ambiguity.

4. RESULTS AND DISCUSSION

FD-OCT images of simple, non-scattering, multi-surface samples and of biological samples were obtained using the harmonic detection method. In this case, a free-space interferometer was used. Figure 2 shows cross-sectional FD-OCT scans of a three-surface test target constructed of a microscope cover slip attached to a mirror through a thin, ~ 100 μm spacer. The sample is tilted with respect to the probe beam to provide a clear idea of the expected locations of the complex conjugate image components. The image in Fig. 2a is obtained by applying the Fourier transform to the complex interferograms acquired using the two-harmonic method. For comparison, Fig. 2b shows the image obtained from the real part of the interferogram, *i.e.*, the image obtainable by conventional FD-OCT which detects real valued interferograms. Figure 3 shows representative A-scans (indicated by the arrows in fig. 2) of this sample obtained using (a) the full complex spectral interferogram and (b) only the real part of the interferogram.

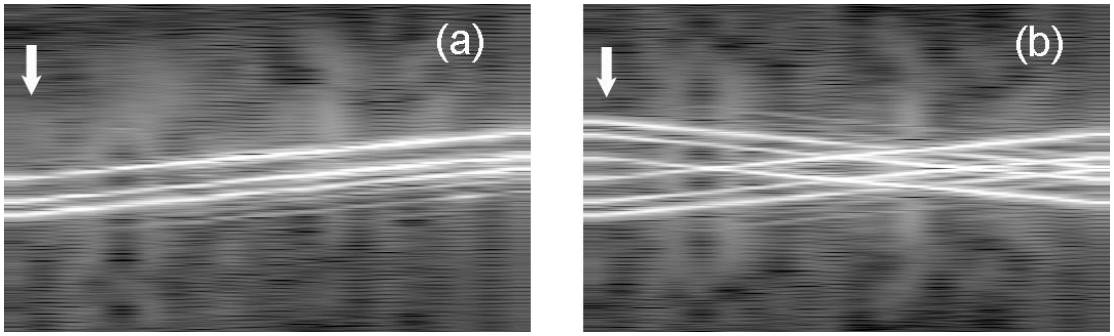

Fig. 2 (a) Complex FD-OCT image of a three-surface object constructed of a glass cover slip and mirror. The harmonic detection method was used to acquire both the imaginary and real spectral interferograms. (b) FD-OCT image resulting from only the real valued interferograms. The arrows indicate the positions of the A-scans shown in fig. 3.

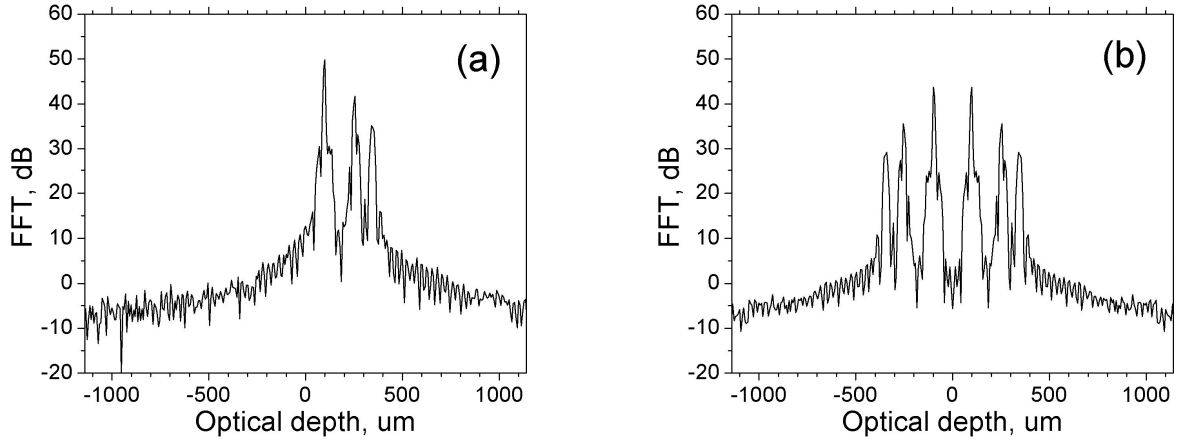

Fig. 3 Time domain depth profiles (A-scans) resulting from inverse Fourier transform of (a) the complex spectral interferogram and (b) the real-valued spectral interferogram. These A-scans correspond to the position of the arrow in fig. 2. The complex conjugate peaks evident in (b) are removed in (a) to the noise level.

Figure 4 shows harmonic FD-OCT transverse cross-sectional images of a region of a tadpole's head. In this case, a fiber-optic interferometer was used. The zero plane is placed slightly below the dorsal (top) surface of the tadpole's head. The images shown on the left and right panels are obtained using the full complex spectral interferograms and only the real interferograms, respectively. The eyes, optic nerves, brain, and other features of the internal structure of the animal are clearly visible. The images in figs. 2 and 4 show that the two-harmonic FD-OCT method can produce clean rejection of the complex conjugate artifact.

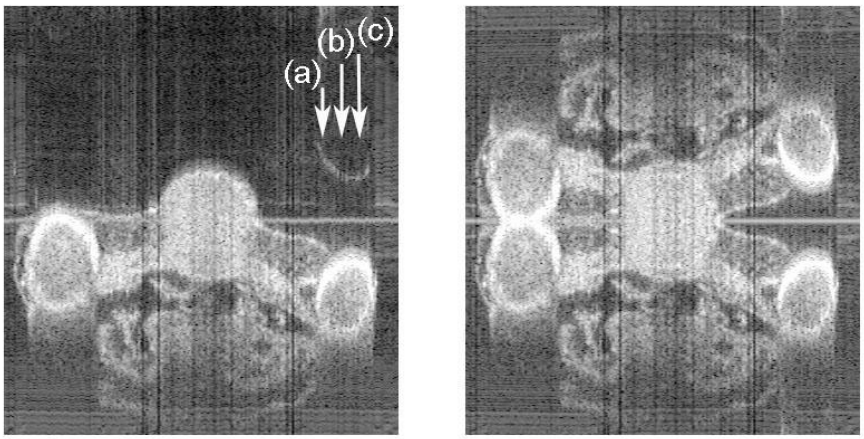

Fig. 4. FD-OCT cross-sectional transverse images from within the head of a fixed, stage 45 *X. tropicalis* tadpole obtained from complex spectral interferograms (left panel) and the real parts of the spectral interferograms (right panel). Light entered from the dorsal surface (top of image). Arrows labeled (a), (b), and (c) indicate A-scans shown in Fig. 5.

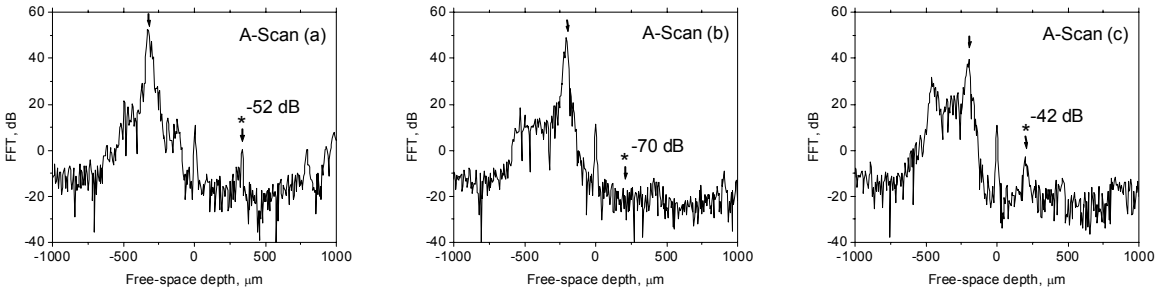

Fig. 5. A-scans indicated in Fig. 4. On each plot, arrows indicate the strongest peak and its complex conjugate. The complex conjugate rejection ratios are listed. The DC peaks are visible at zero depth.

Generally, the complex conjugate image is suppressed to the background noise level and is not visible at all. The only exception is the very bright image of the eye on the right side of the image, for which a weak complex conjugate artifact remains. Figure 5 shows representative examples of A-scans that correspond to that area (indicated by the arrows in Fig. 2). The rejection ratio is typically 50–60 dB, and can be as low as 40 dB and as high as 70 dB. We attribute the incomplete rejection, as well as the incompletely rejected DC artifact at the zero phase delay in the tadpole image, to the slow 0.5 Hz A-scan data acquisition used in this experiment in conjunction with the fiber-optic interferometer. This allows phase noise in the fiber optic interferometer to affect the measurements. (The dc term is fully rejected when the free-space interferometer is used; see figs. 2 and 3.) We expect that improvement can be achieved by using faster data acquisition (*e.g.*, by using a faster linear array detector or a swept-source OCT instrument) and consistently obtain at least 70 dB rejection.

In summary, we have presented a simple harmonic detection method for obtaining full, complex spectral interferograms and removing the complex conjugate ambiguity in FD-OCT. Images of a tadpole show applicability of this method to biological samples. The complex conjugate, dc, or autocorrelation artifacts can be rejected to the background noise level. Implementation of the two-harmonic method for swept-source FD-OCT should be straightforward. With broadband FD-OCT, high-speed data acquisition can be achieved using sampling of the spectral interferograms with a high speed integrating linear array detector while phase modulating the interferometer, followed by digital lock-in filtering. Future work will apply harmonic detection to swept source OCT. We believe our method will be useful for a variety of biomedical low coherence optical imaging applications including its application to the development of spectroscopic FD-OCT.

This work was supported by the National Institutes of Health.

REFERENCES

1. R. A. Leitgeb, C. K. Hitzenberger, and A. F. Fercher, "Performance of Fourier domain *vs.* time domain optical coherence tomography," *Opt. Express* 11, 889 (2003).
2. M. A. Choma, M. V. Sarunic, C. Yang, and J. A. Izatt, "Sensitivity advantage of swept source and Fourier domain optical coherence tomography," *Opt. Express* 11, 2183 (2003).
3. J. F. de Boer, B. Cense, B. H. Park, M. C. Pierce, G. J. Tearney, and B. E. Bouma, "Improved signal-to-noise ratio in spectral-domain compared with time-domain optical coherence tomography," *Opt. Lett*. 28, 2067 (2003).
4. R. Leitgeb, M. Wojtkowski, A. Kowalczyk, C. K. Hitzenberger, M. Sticker, and A. F. Fercher, "Spectral measurement of absorption by spectroscopic frequency-domain optical coherence tomography," *Opt. Lett*. 25, 820 (2000).
5. C. Xu, C. Vinegoni, T. S. Ralston, W. Luo, W. Tan, and S. A. Boppart, "Spectroscopic spectral-domain optical coherence tomography," *Opt. Lett*. 31, 1079 (2006).

6. U. Morgner, W. Drexler, F. X. Kartner, X. D. Li, C. Pitris, E. P. Ippen, and J. G. Fujimoto, "Spectroscopic optical coherence tomography," *Opt. Lett.* 25, 111 (2000).
7. P. Hariharan, B. F. Oreb, and T. Eiju, "Digital phase-shifting interferometry: a simple error-compensating phase calculation algorithm," *Appl. Opt.* 26, 2504 (1987).
8. J. Schmit and K. Creath, "Extended averaging technique for derivation of error-compensating algorithms in phase-shifting interferometry," *Appl. Opt.* 34, 3610 (1995).
9. M. Wojtkowski, A. Kowalczyk, R. Leitgeb, and A. F. Fercher, "Full range complex spectral optical coherence tomography technique in eye imaging," *Opt. Lett.* 27, 1415 (2002).
10. R. A. Leitgeb, C. K. Hitzenberger, A. F. Fercher, and T. Bajraszewski, "Phase-shifting algorithm to achieve high-speed long-depth-range probing by frequency-domain optical coherence tomography," *Opt. Lett.* 28, 2201 (2003).
11. M. A. Choma, C. Yang, and J. A. Izatt, "Instantaneous quadrature low-coherence interferometry with 3x3 fiber-optic couplers," *Opt. Lett.* 28, 2162 (2003).
12. M. V. Sarunic, B. E. Applegate and J. A. Izatt, "Real-time quadrature projection complex conjugate resolved Fourier domain optical coherence tomography," *Opt. Lett.*313, 2426 (2006).
13. J. Zhang, J. S. Nelson, and Z. Chen, "Removal of a mirror image and enhancement of the signal-to-noise ratio in Fourier-domain optical coherence tomography using an electro-optic phase modulator," *Opt. Lett.* 30, 147 (2005).
14. 14. S. H. Yun, G. J. Tearney, J. F. de Boer, and B. E. Bouma, "Removing the depth-degeneracy in optical frequency domain imaging with frequency shifting," *Opt. Express* 12, 4822 (2004).
15. A. M. Davis, M. A. Choma, and J. A. Izatt, "Heterodyne swept-source optical coherence tomography for complete complex conjugate ambiguity removal," *J. Biomed. Opt.* 10, 064005 (2005).
16. B. J. Vakoc, S. H. Yun, G. J. Tearney, and B. E. Bouma, "Elimination of depth degeneracy in optical frequency-domain imaging through polarization-based optical demodulation," *Opt. Lett.* 31, 362 (2006).
17. G.-S. Han and S.-W. Kim, "Numerical correction of reference phases in phase-shifting interferometry by iterative least-squares fitting," *Appl. Opt.* 33, 7321 (1994).
18. P. Targowski, I. Gorczynska, M. Szkulmowski, M. Wojtkowski, and A. Kowalczyk, "Improved complex spectral domain OCT for in vivo eye imaging," *Opt. Commun.* 249, 357 (2005).
19. A. B. Vakhtin, K. A. Peterson, and D. J. Kane, "Resolving the complex conjugate ambiguity in Fourier domain OCT by harmonic lock-in detection of the spectral interferogram," *Opt. Lett.* 31, 1271 (2006).